

# SoPE: Spherical Coordinate-Based Positional Embedding for Enhancing Spatial Perception of 3D LVLMs

Guanting Ye<sup>1</sup> Qiyao Zhao<sup>3</sup> Wenhao Yu<sup>2</sup> Liangyu Yuan<sup>4</sup> Mingkai Li<sup>5</sup> Xiaofeng Zhang<sup>3</sup>  
 Jianmin Ji<sup>2</sup> Yanyong Zhang<sup>2</sup> Qing Jiang<sup>4</sup> Ka-Veng Yuen<sup>1</sup>

<sup>1</sup>University of Macau <sup>2</sup>University of Science and Technology of China

<sup>3</sup>Shanghai Jiaotong University <sup>4</sup>Hefei University of Technology <sup>5</sup>National University of Singapore

Corresponding author: kvu@um.edu.mo

## Abstract

3D Large Vision-Language Models (3D LVLMs) built upon Large Language Models (LLMs) have achieved remarkable progress across various multimodal tasks. However, their inherited position-dependent modeling mechanism, Rotary Position Embedding (RoPE), remains suboptimal for 3D multimodal understanding. The vanilla RoPE formulation fails to preserve essential three-dimensional spatial structures when encoding 3D tokens, and its relative distance computation overlooks angular dependencies hindering the model’s ability to capture directional variations in visual representations. To overcome these limitations, we introduce Spherical Coordinate-based Positional Embedding (SoPE). Our method maps point-cloud token indices into a 3D spherical coordinate space, enabling unified modeling of spatial locations and directional angles. This formulation preserves the inherent geometric structure of point-cloud data, enhances spatial awareness, and yields more consistent and expressive geometric representations for multimodal learning. In addition, we introduce a multi-scale frequency mixing strategy to fuse feature information across different frequency domains. Experimental results on multiple 3D scene benchmarks validate the effectiveness of our approach, while real-world deployment experiments further demonstrate its strong generalization capability.

## 1. Introduction

Three-dimensional scenes are the physical substrate of everyday interaction, and enabling machines to perceive, reason about, and act within them is a central goal in AI. Recent efforts build 3D Large Vision-Language Models (LVLMs) [1, 8, 10, 26, 66, 81, 88, 89] that leverage pretrained LLMs to lift 3D scene understanding from geometric recognition toward richer semantic, functional, and intent-aware reasoning. To construct 3D visual fea-

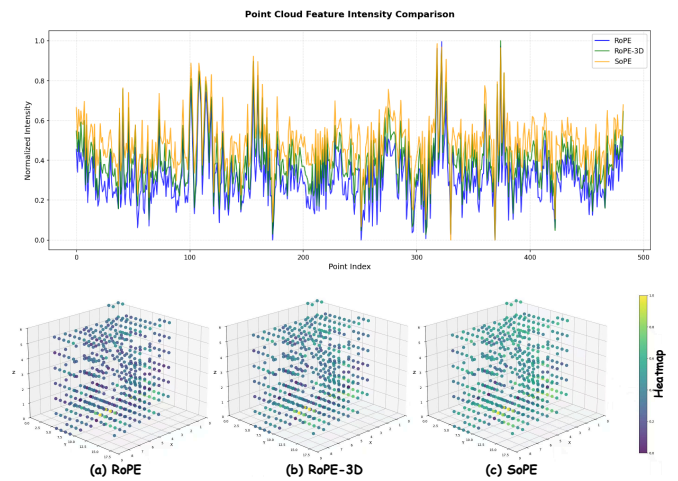


Figure 1. **SoPE enhances 3D spatial representation via geometry-aware positional encoding.** Conventional positional encoding methods such as (a) RoPE and (b) RoPE-3D exhibit spatial perception bias: cross-modal attention concentrates on a few hotspots and fails to capture global context, resulting in less discriminative spatial features. In contrast, the proposed (c) SoPE produces more balanced and global attention patterns while amplifying spatial feature saliency, indicating a deeper understanding of the 3D environment.

tures that can interface with language, prior work has followed several routes: projecting point clouds into images [13, 21, 23, 24, 57, 83], directly encoding 3D geometry [4, 33, 51, 58, 60, 65, 77, 90], or fusing multi-view images [11, 18, 25, 47, 48, 62] and point clouds as in LLaVA-3D [86]. These advances focus on the visual front end, but successful end-to-end 3D LVLMs also require connectors that preserve spatial and pose cues when aligning visual tokens to the LLM input space.

Unlike the most prior work, we take a positional-encoding perspective and focus on rotary positional embedding (RoPE) [22, 49], which is widely adopted for position-

dependent modeling in current 3D LVLMs. RoPE flattens point-cloud tokens into a 1D sequence in raster order and assigns positional indices according to their sequence positions, modeling positional dependencies via relative index differences. While this design is effective in NLP, in 3D settings it relies solely on 1D sequence indices to implicitly represent geometry and thus ignores the inherent 3D attributes of point-cloud tokens, such as their true spatial locations and orientations. This mismatch between the index-based positional modeling and the underlying point-cloud geometry breaks 3D neighborhood continuity and weakens the model’s ability to capture spatial relations and directional variations. As illustrated in Figure. 1, cross-modal attention collapses onto a few hotspots, many 3D tokens with clearly different positions and orientations receive nearly identical attention weights, and large regions of the scene are effectively ignored, resulting in pronounced spatial perception bias.

Although recent efforts have extended RoPE from 1D temporal position modeling to multimodal settings, these methods are primarily tailored to images or videos and do not align well with the characteristics of point-cloud tokens [22, 31, 52, 59]. While these approaches substantially improve the behavior of RoPE in their respective settings, they still treat positional indices as sequence- or grid-based and do not explicitly encode the 3D geometric structure of point-cloud tokens in 3D LVLMs. Motivated by the sub-optimal behavior observed in Figure. 1, we further analyze RoPE from an internal modeling perspective and attribute its key limitations in encoding point-cloud token positions to the following two factors:

**Finding:** (i) *RoPE fails to preserve essential 3D spatial structure when modeling positions of 3D tokens.* (ii) *RoPE’s relative position term is direction-agnostic and cannot capture orientation changes.*

- We propose SoPE, a connector-level positional encoding for 3D LVLMs that remaps 3D tokens from a 1D raster index to a spherical tuple  $(t, r, \theta, \phi)$ , and redistributes RoPE frequency bands with multi-scale phase mixing so that temporal order, depth, and orientation are encoded in a geometry-consistent, direction-aware way.
- Plugged into SpatialLM as a drop-in replacement for vanilla RoPE, SpatialSoPE consistently improves 3D layout estimation and object detection across benchmarks and produces more balanced, geometry-aware cross-modal attention patterns.

To validate the practical applicability of our method, we performed an end-to-end deployment on a real device and reported measured metrics such as latency, frame rate, and power consumption.

## 2. Related Work

### 2.1. 3D Large Vision-Language Models

Large multimodal models (LMMs), and in particular large vision-language models (LVLMs), have advanced rapidly, extending large language model (LLM) reasoning to visual and 3D inputs. A common paradigm projects images or 3D representations into the language embedding space so that visual features can be jointly processed with text tokens.

A first line of 3D LVLMs [6–8, 12, 15, 17, 24, 28, 30, 32, 34, 36, 39–42, 54, 55, 65, 67, 73, 75, 85–87] focuses on strengthening 3D visual representations. For example, ScanReason, PointLLM and LL3DA employ dedicated 3D encoders to directly model point-cloud geometry, while Video-3D LVLMs and Scene-LLM extract multi-view image features with 3D awareness; LLaVA-3D further injects point-cloud features into multi-view image tokens to produce 2D tokens enriched with 3D context.

Another line of work advances 3D capability from data, architectural, and memory perspectives. SpatialLM [43] proposes a compound 3D-informed design of data, architectures and training to improve 3D spatial reasoning; Inst3D LMM [70] achieves instance-level 2D–3D fusion and relation modeling via Multi-view Cross-Modal Fusion and 3D-ISR; 3DLLM-MEM [27] equips embodied 3D agents with dynamic working and episodic memory and introduces 3DMEM-BENCH to evaluate long-term spatiotemporal memory. LSceneLLM [84] leverages LLM visual preferences [19] to guide a scene magnifier with adaptive attention, refining representations from sparse to fine-grained for cross-room scenes and introducing the XR-Scene benchmark.

### 2.2. Position Encoding Schemes in LMMs

Most 3D LMMs adopt the RoPE commonly used in LLMs: they flatten images into 1D tokens in raster order and apply complex phase rotations in the embedding space. This approach, however, breaks spatial neighborhood continuity, introduces end of sequence bias along the temporal dimension, and causes attention dilution as views and frames increase. To address these issues, various 2D image and video improvements have been proposed: HoPE [9] selectively preserves high frequency components; CoMemo [38] and MiniCPM-V [71] design RoPE variants to mitigate long range attenuation; CCA [80] and MCA [80] use heuristic index assignments to reduce hallucinations in long sequences; and VideoRoPE [59], M-RoPE [56] and decompose positional embeddings into 1D, 2D, and 3D components with hierarchical frequency distributions to improve spatiotemporal performance. New ideas for multi view and 3D sequences are also emerging: ComRoPE [69] uses a trainable exchangeable angle matrix to improve scaling and robustness; FoPE [29] restores spectral damage in the fre-

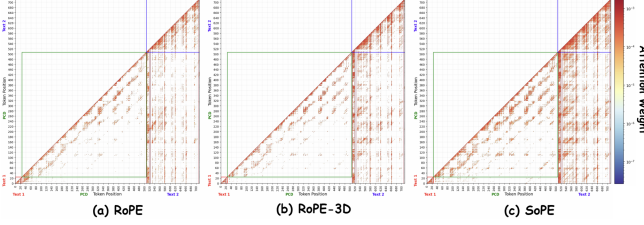


Figure 2. **Comparison of cross-modal attention patterns with RoPE, RoPE-3D, and SoPE.** (a) With RoPE, attention is predominantly intra-modal, failing to establish effective connections between the text and the point cloud. (b) RoPE-3D yields marginal improvements in cross-modal attention but remains limited. (c) The proposed SoPE successfully establishes stronger cross-modal attention links and substantially enhances information flow between the two modalities.

quency domain to enhance long sequence generalization; DRoPE [79] adds Directionality to RoPE to handle heading periodicity; CR2PQ [76] leverage two view 3D priors to improve matching and geometric reconstruction. And Circle-RoPE [53] introduces a cone-like geometric projection to decouple cross-modal positional encodings. Overall, despite a range of effective strategies, a systematic unified positional encoding scheme for multi view, long temporal 3D sequences remains lacking and warrants further study.

### 3. Motivation and Analysis

In this section, we provide an overview of the architecture of baseline 3D LVLMs and explain how RoPE is applied within them. Furthermore, through information flow analysis, we reveal the negative impact of RoPE on multimodal understanding, which forms a strong foundation for our proposed design.

#### 3.1. Preliminary

**3D LVLMs.** We adopt SpatialLM [45] as our baseline 3D LVM, denoted by  $\mathcal{F}$ . It is composed of three key components: a point cloud encoder  $\mathcal{F}_p$ , a large language model (LLM)  $\mathcal{F}_t$ , and a projector  $f$  designed to map point cloud embeddings into the text embedding space. Given a point cloud input  $I_p$  and a textual prompt input  $I_t$ , the model  $\mathcal{F}$  encodes them into a multimodal sequence  $\mathcal{S} = \{\mathcal{S}_p, \mathcal{S}_t\}$ , where  $\mathcal{S}_p = f(\mathcal{F}_p(I_p)) = \{w_m\}_{m=1}^P$  and  $\mathcal{S}_t = \mathcal{F}_t(I_t) = \{w_m\}_{m=1}^T$  represent point cloud and text tokens of lengths  $V$  and  $T$ , respectively.

**Rotary Position Encoding.** As the 3D multimodal successor of LLMs, SpatialLM inherits RoPE to encode the relative positional information of each token  $w_m$ . Specifically, given a query token  $Q_{t_1}$  at position  $t_1$  and a key token  $K_{t_2}$  at position  $t_2$ , both with the same dimension  $d$ , RoPE divides the dimension  $d$  into  $d/2$  pairs, with each pair assigned pre-

defined sinusoidal function values

$$\left\{ \theta'_i = 10000^{-2(i-1)/d} \right\}, \quad i \in \{1, 2, \dots, d/2\},$$

where  $\theta'_i$  denote the RoPE base angles. Subsequently, the rotation matrix  $r^{(i)}$  is constructed as

$$r^{(i)} = \begin{pmatrix} \cos(\theta'_i) & -\sin(\theta'_i) \\ \sin(\theta'_i) & \cos(\theta'_i) \end{pmatrix} \quad (1)$$

The relative rotation matrix  $R_{\Delta t}$  is defined as  $R_{\Delta t} = \text{diag}(\Delta t r^{(1)}, \dots, \Delta t r^{(d/2)})$ , where  $\Delta t$  denotes the relative positional distance. The vanilla RoPE uses  $d = 128$  and encodes the relative positional relationship between  $Q_{t_1}$  and  $K_{t_2}$  through the following relative matrix:

$$\begin{pmatrix} Q^{(0)} \\ Q^{(1)} \\ \vdots \\ Q^{(126)} \\ Q^{(127)} \end{pmatrix}^\top \begin{pmatrix} \cos \theta'_0 \Delta t & -\sin \theta'_0 \Delta t & \cdots & 0 & 0 \\ \sin \theta'_0 \Delta t & \cos \theta'_0 \Delta t & \cdots & 0 & 0 \\ \vdots & \vdots & \ddots & \vdots & \vdots \\ 0 & 0 & \cdots & \cos \theta'_{63} \Delta t & -\sin \theta'_{63} \Delta t \\ 0 & 0 & \cdots & \sin \theta'_{63} \Delta t & \cos \theta'_{63} \Delta t \end{pmatrix} \begin{pmatrix} K^{(0)} \\ K^{(1)} \\ \vdots \\ K^{(126)} \\ K^{(127)} \end{pmatrix} \quad (2)$$

#### 3.2. Spatial Perception Bias

We conduct an in-depth analysis of the spatial perception bias introduced by RoPE through information flow visualization, revealing its negative impact on 3D multimodal understanding. Finally, we clarify the limitations of RoPE’s positional modeling mechanism and attribute the spatial perception bias to deficiencies in positional indexing and relative distance computation.

**Information flow for Spatial Perception Bias.** We visualize the information flow from the point cloud to the textual prompt to examine the spatial perception bias caused by RoPE. As shown in Figure 2, we observe that most 3D point cloud tokens exhibit sparse information flow. This indicates an uneven perception of visual features in 3D space by textual tokens during cross-modal interaction, where only a subset of point cloud tokens receive high attention. We refer to this phenomenon as spatial perception bias. Beyond the global hotspot pattern, we further observe that small objects and structural boundaries in large indoor scenes are often suppressed: their corresponding 3D tokens receive almost uniformly low attention even when they are geometrically and semantically salient. This suggests that a single positional scale in RoPE is not sufficiently sensitive to small angular variations and local geometric changes. In the following, we attribute the causes of spatial perception bias to two key limitations from the perspective of position-dependent modeling.

**Hard embedding of 3D point cloud tokens.** The 3D point cloud tokens are flattened into a one-dimensional sequence

<sup>1</sup>To avoid confusion with the polar angle  $\theta$  used later in spherical coordinates, we denote the RoPE base angles as  $\theta'_i$ .

and assigned positional indices following a raster-scan order. Although this approach is straightforward, it neglects the inherent difference between the spatial continuity of point cloud features and the discreteness of textual features, thereby disrupting the locality of three-dimensional spatial structures. In particular, spatially adjacent point cloud tokens are assigned non-adjacent positional indices.

**Temporal-dependent relative position computation.** In RoPE, the relative distance between the query token  $Q_{t_1}$  and the key token  $K_{t_2}$  is computed as follows:

$$\Delta t = t_1 - t_2. \quad (3)$$

This distance computation can only capture the temporal variation of 3D tokens within the sequence. Standard RoPE is inherently unaware of the actual spatial position changes of tokens, a problem that recent variants like 3D-RoPE attempt to address by mapping visual tokens into spatial coordinates. However, these methods still fail to perceive crucial directional variations in visual representations, which is a key attribute of spatial awareness. Our proposed method directly targets this remaining gap.

The two aforementioned limitations form a solid foundation for our design. To address them, we propose a Spherical Coordinate-Based Positional Embedding to enhance the model’s perception of global spatial information. Inspired by prior 2D LVLMs that assign two-dimensional coordinates to image tokens to provide spatial cues, we further explore a simple RoPE variant that assigns three-dimensional coordinates to 3D tokens, referred to as RoPE-3D, which serves as a comparative baseline for our method.

## 4. Method

We propose Spherical Coordinate-Based Positional Embedding (SoPE), a positional encoding variant tailored to 3D point-cloud tokens. As illustrated in Figure 3, SoPE reparameterizes point-cloud tokens from Cartesian coordinates into a spherical coordinate system, enhancing the model’s sensitivity to both spatial positions and directional variations. SoPE comprises three key components: spherical coordinate positional projection, multi-dimensional frequency allocation, and multi-scale frequency encoding.

### 4.1. Spherical Coordinate Positional Projection

Spherical coordinate positional projection, decouples 3D spatial tokens from the 1D textual sequence by replacing the flattened raster index with a geometry-aware tuple  $(t, r, \theta, \phi)$ . This process comprises two key steps:

(i) **Positional Index Reallocation:** We extract the Cartesian coordinates  $(x, y, z)$  of point cloud tokens to represent their intrinsic 3D spatial positions, while preserving the original RoPE-assigned index  $t$  to maintain their temporal ordering within the sequence. Each token is thereby

assigned a reallocated four-dimensional positional index  $(t, x, y, z)$ , integrating both sequential and spatial information for unified positional encoding.

(ii) **Spherical Coordinate Mapping:** We project the Cartesian positional index components into a spherical coordinate space, where the three spherical components radius  $r$ , polar angle  $\theta$ , and azimuthal angle  $\phi$  are computed as follows:

$$\begin{aligned} r &= \sqrt{x^2 + y^2 + z^2}, \\ \theta &= \arccos\left(\frac{z}{r}\right), \\ \phi &= \text{atan2}(y, x). \end{aligned} \quad (4)$$

We then combine the temporal index  $t$  with the three spherical components to obtain the final composite four-dimensional positional index  $(t, r, \theta, \phi)$ . Finally, we effectively embed both spatial location and angular orientation of point cloud tokens into the positional modeling scheme. Building upon this enriched representation, we further generalize RoPE’s original relative position formulation (Equation 3) by decomposing the displacement across all four components:

$$\begin{aligned} \Delta t &= t_1 - t_2, & \Delta r &= r_1 - r_2, \\ \Delta \theta &= \theta_1 - \theta_2, & \Delta \phi &= \phi_1 - \phi_2. \end{aligned} \quad (5)$$

This extended formulation enables the model to capture spatial and directional variations when computing relative positional relationships between point cloud tokens.

### 4.2. Multi-dimensional Frequency Allocation

In Sec. 4.1, we extend the temporal positional index to include four components: temporal position  $t$ , radius  $r$ , polar angle  $\theta$ , and azimuthal angle  $\phi$ . In this work we split the frequency spectrum into four proportional parts corresponding to these components, with an allocation ratio  $t : r : \theta : \phi = 24 : 2 : 3 : 3$ . To determine this design we ran extensive ablation experiments comparing many alternative allocations and band-orderings; the results guided our choice of both the per-component bandwidths and the subband ordering used in the final model. Concretely, we map the three spherical-coordinate components  $r, \theta, \phi$  to the front higher-frequency subbands and place the temporal component  $t$  in the later lower-frequency subbands. Intuitively, assigning the spherical components to higher frequencies helps the model capture fine-grained spatial and angular variations and directional cues, while allocating a larger low-frequency block to the temporal component preserves slower, long-range temporal dynamics and continuity. This allocation achieved the best trade-off between spatial and angular resolution and temporal coherence in our ablation studies. The final relative rotation matrix is formulated as follows:

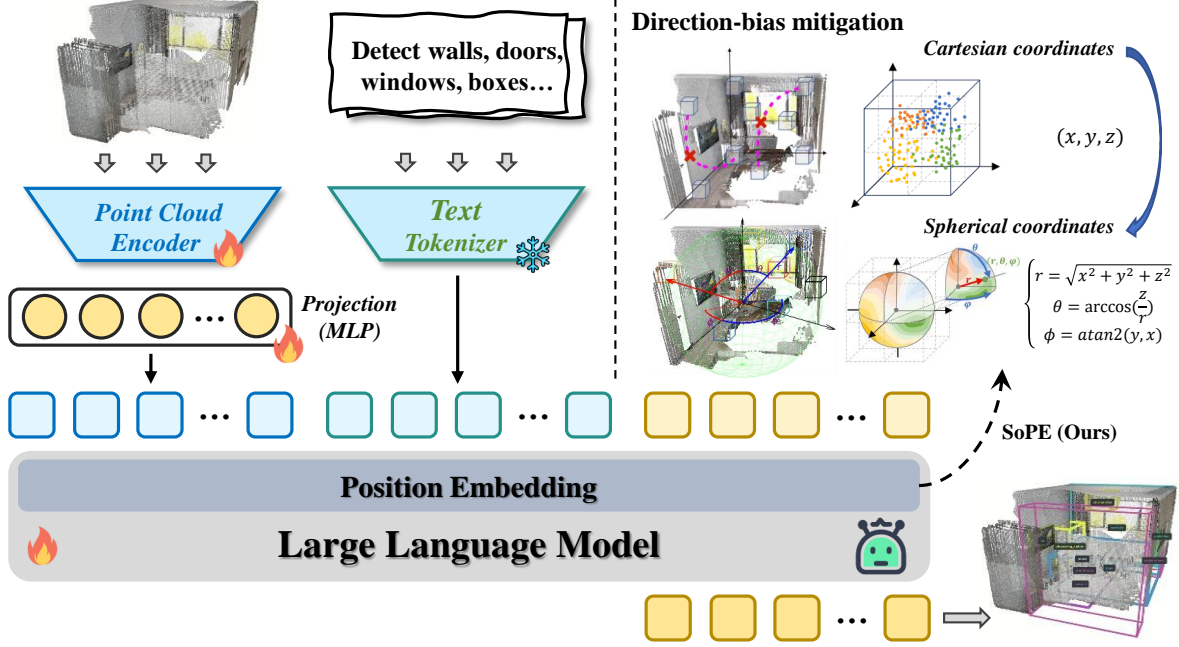


Figure 3. SoPE: Spherical Coordinate-Based Positional Embedding for Multimodal 3D Scene Understanding. The figure illustrates the overall SpatialSoPE framework, where SoPE is integrated into SpatialLM. By transforming coordinates from Cartesian to spherical, SpatialSoPE mitigates spatial directional bias and enables more robust 3D object understanding and localization.

$$\begin{aligned}
 & \begin{pmatrix} Q^{(0)} \\ Q^{(1)} \\ Q^{(2)} \\ Q^{(3)} \\ \vdots \\ Q^{(6)} \\ Q^{(7)} \end{pmatrix}^T \begin{pmatrix} \cos \theta'_6 \Delta r & -\sin \theta'_6 \Delta r & 0 & \dots & 0 & 0 \\ \sin \theta'_6 \Delta r & \cos \theta'_6 \Delta r & 0 & \dots & 0 & 0 \\ 0 & 0 & \cos \theta'_1 \Delta r & -\sin \theta'_1 \Delta r & \dots & 0 \\ 0 & 0 & \sin \theta'_1 \Delta r & \cos \theta'_1 \Delta r & \dots & 0 \\ \vdots & \vdots & \vdots & \vdots & \ddots & \vdots \\ 0 & 0 & \dots & 0 & \cos \theta'_5 \Delta r & -\sin \theta'_5 \Delta r \\ 0 & 0 & \dots & 0 & \sin \theta'_5 \Delta r & \cos \theta'_5 \Delta r \end{pmatrix} \begin{pmatrix} K^{(0)} \\ K^{(1)} \\ K^{(2)} \\ K^{(3)} \\ \vdots \\ K^{(6)} \\ K^{(7)} \end{pmatrix} \\
 + & \begin{pmatrix} Q^{(8)} \\ Q^{(9)} \\ Q^{(10)} \\ Q^{(11)} \\ \vdots \\ Q^{(18)} \\ Q^{(19)} \end{pmatrix}^T \begin{pmatrix} \cos \theta'_1 \Delta \theta & -\sin \theta'_1 \Delta \theta & 0 & \dots & 0 & 0 \\ \sin \theta'_1 \Delta \theta & \cos \theta'_1 \Delta \theta & 0 & \dots & 0 & 0 \\ 0 & 0 & \cos \theta'_5 \Delta \theta & -\sin \theta'_5 \Delta \theta & \dots & 0 \\ 0 & 0 & \sin \theta'_5 \Delta \theta & \cos \theta'_5 \Delta \theta & \dots & 0 \\ \vdots & \vdots & \vdots & \vdots & \ddots & \vdots \\ 0 & 0 & \dots & 0 & \cos \theta'_9 \Delta \theta & -\sin \theta'_9 \Delta \theta \\ 0 & 0 & \dots & 0 & \sin \theta'_9 \Delta \theta & \cos \theta'_9 \Delta \theta \end{pmatrix} \begin{pmatrix} K^{(8)} \\ K^{(9)} \\ K^{(10)} \\ K^{(11)} \\ \vdots \\ K^{(18)} \\ K^{(19)} \end{pmatrix} \\
 + & \begin{pmatrix} Q^{(20)} \\ Q^{(21)} \\ Q^{(22)} \\ Q^{(23)} \\ \vdots \\ Q^{(30)} \\ Q^{(31)} \end{pmatrix}^T \begin{pmatrix} \cos \theta'_{10} \Delta \phi & -\sin \theta'_{10} \Delta \phi & 0 & \dots & 0 & 0 \\ \sin \theta'_{10} \Delta \phi & \cos \theta'_{10} \Delta \phi & 0 & \dots & 0 & 0 \\ 0 & 0 & \cos \theta'_{11} \Delta \phi & -\sin \theta'_{11} \Delta \phi & \dots & 0 \\ 0 & 0 & \sin \theta'_{11} \Delta \phi & \cos \theta'_{11} \Delta \phi & \dots & 0 \\ \vdots & \vdots & \vdots & \vdots & \ddots & \vdots \\ 0 & 0 & \dots & 0 & \cos \theta'_{15} \Delta \phi & -\sin \theta'_{15} \Delta \phi \\ 0 & 0 & \dots & 0 & \sin \theta'_{15} \Delta \phi & \cos \theta'_{15} \Delta \phi \end{pmatrix} \begin{pmatrix} K^{(20)} \\ K^{(21)} \\ K^{(22)} \\ K^{(23)} \\ \vdots \\ K^{(30)} \\ K^{(31)} \end{pmatrix} \\
 + & \begin{pmatrix} Q^{(32)} \\ Q^{(33)} \\ Q^{(34)} \\ Q^{(35)} \\ \vdots \\ Q^{(126)} \\ Q^{(127)} \end{pmatrix}^T \begin{pmatrix} \cos \theta'_{16} \Delta t & -\sin \theta'_{16} \Delta t & 0 & \dots & 0 & 0 \\ \sin \theta'_{16} \Delta t & \cos \theta'_{16} \Delta t & 0 & \dots & 0 & 0 \\ 0 & 0 & \cos \theta'_{17} \Delta t & -\sin \theta'_{17} \Delta t & \dots & 0 \\ 0 & 0 & \sin \theta'_{17} \Delta t & \cos \theta'_{17} \Delta t & \dots & 0 \\ \vdots & \vdots & \vdots & \vdots & \ddots & \vdots \\ 0 & 0 & \dots & 0 & \cos \theta'_{63} \Delta t & -\sin \theta'_{63} \Delta t \\ 0 & 0 & \dots & 0 & \sin \theta'_{63} \Delta t & \cos \theta'_{63} \Delta t \end{pmatrix} \begin{pmatrix} K^{(32)} \\ K^{(33)} \\ K^{(34)} \\ K^{(35)} \\ \vdots \\ K^{(126)} \\ K^{(127)} \end{pmatrix} \quad (6)
 \end{aligned}$$

The matrices in Equations (6) are finally integrated into the overall rotation matrix.

### 4.3. Multi-scale Frequency Mixing Strategy

Single-scale positional encodings, even with spherical coordinates, struggle to capture both fine-grained geometry and

large-scale architectural layouts in indoor 3D scenes, which motivates a multi-scale treatment of positional cues. To this end, we introduce a multi-scale frequency mixing strategy at the positional phase level. For each temporal or spherical coordinate component  $u \in \{t, r, \theta, \phi\}$ , we regard  $u$  as a fixed geometric quantity and define different *scales* as deterministic transforms applied to the same  $u$  before RoPE phase computation. Concretely, we construct three complementary coordinate transforms  $g^{\text{lin}}(u)$ ,  $g^{\text{log}}(u)$ , and  $g^{\text{per}}(u)$ , corresponding to a linear scale that preserves absolute positional precision, a log-compressed scale that emphasizes local neighborhood structure, and a periodic scale that captures global patterns and long-range dependencies.

In practice, multi-scale fusion is implemented directly at the RoPE phase level. For each frequency band  $k$  assigned to component  $u$ , the final phase used in the  $k$ -th rotation block is:

$$\varphi_k(u) = \frac{1}{3} \left( \omega_k^{\text{lin}} g^{\text{lin}}(u) + \omega_k^{\text{log}} g^{\text{log}}(u) + \omega_k^{\text{per}} g^{\text{per}}(u) \right), \quad (7)$$

where  $\omega_k$  denote the RoPE base frequencies at each scale. We use fixed uniform weights across the three scales without introducing additional learnable parameters, keeping the design lightweight while still yielding clear gains in our ablation studies. By mixing phases across scales in this manner, SoPE can simultaneously encode precise locations, local context, and global 3D structure, leading to more balanced attention patterns and stronger cross-modal links.

Table 1. **Integration of SoPE enables state-of-the-art layout estimation.** Our results indicate that the SpatialSoPE module, when fine-tuned (ft), is the main factor enabling us to outperform prior methods such as RoomFormer and SceneScript.

Methods	F1 - Structured3D	
	IoU <sub>2D</sub> @0.25↑	IoU <sub>2D</sub> @0.5↑
RoomFormer [74]	70.4	67.2
SceneScript [2]	83.1	80.8
SpatialLM (ft. Structured3D) [45]	32.8	17.9
SpatialSoPE (ft. Structured3D)	33.5	29.5
SpatialLM (ft. SpatialLM Dataset → Structured3D)	86.5	84.6
SpatialSoPE (ft. SpatialLM Dataset) → Structured3D)	<b>88.7</b>	<b>86.2</b>

Table 2. **3D object detection results on the ARKitScenes dataset.** SpatialSoPE consistently outperforms SpatialLM and other 3D LVLM baselines.

Methods	F1 - ARKitScenes	
	IoU <sub>3D</sub> @0.25↑	IoU <sub>3D</sub> @0.50↑
VoteNet [14]	53.9	45.4
H3DNet [78]	55.7	46.3
NeRF-Det [64]	60.3	34.7
UniDet3D [35]	62.8	48.3
SpatialLM [45]	63.9	60.7
SpatialSoPE	<b>66.1</b>	<b>63.2</b>

Table 3. **Comparison between SpatialSoPE and SpatialLM on the SpatialLM Dataset and Structured3D.** SpatialSoPE consistently outperforms the SpatialLM baseline across all metrics on both datasets.

Methods	F1 - SpatialLM Dataset		F1 - Structured3D	
	IoU <sub>3D</sub> @0.25↑	IoU <sub>3D</sub> @0.50↑	IoU <sub>3D</sub> @0.25↑	IoU <sub>3D</sub> @0.50↑
SpatialLM [45]	69.7	62.0	31.8	17.6
SpatialSoPE	<b>71.4</b>	<b>63.4</b>	<b>33.3</b>	<b>17.9</b>

## 5. Experiment

### 5.1. Experimental Setup

Following SpatialLM [45], we adopt Sonata [61] as the point cloud encoder and train it jointly with the rest of the model. Qwen2.5-0.5B [68] as the LLM, and a two-layer MLP [5, 16] to bridge the two modules. All experiments are conducted in a single-stage training setup using four NVIDIA H20 GPUs. We evaluate our method on three 3D scene benchmarks for layout estimation and 3D object detection. We adopt IoU<sub>2D</sub> as the metric for layout estimation and IoU<sub>3D</sub> for 3D object detection [45]. For all ablation studies, we keep the experimental settings and test splits identical to the original SpatialLM setup to ensure fair comparisons. SpatialSoPE denotes SpatialLM equipped with the proposed SoPE positional encoding.

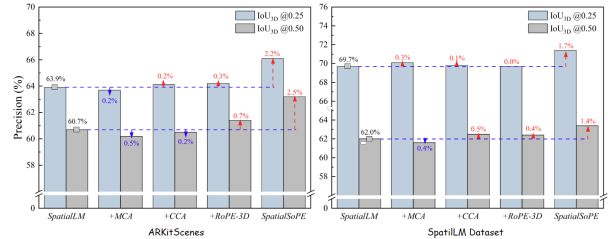


Figure 4. **Effectiveness of the SoPE module demonstrated through component analysis.** The figure compares various components added to the SpatialLM, highlighting the superior contribution of SoPE to model precision. Results are shown for (a) the ARKitScenes and (b) the SpatialLM datasets.

### 5.2. Experimental comparison results.

**Results of Layout Estimation.** The layout estimation task tests a model’s 3D spatial perception by predicting architectural elements in indoor scenes. On Structured3D, SpatialSoPE reaches IoU<sub>2D</sub>@0.25 and IoU<sub>2D</sub>@0.5 of 88.7 and 86.2, achieving gains of +2.2 and +1.6 over SpatialLM (Table 1). We observe consistent improvements under both training-from-scratch and pretrain-then-finetune configurations, indicating that the geometry- and direction-aware positional cues of SoPE are robust across training protocols and data scales.

**Results of 3D Object Detection.** We further evaluate SpatialSoPE on three 3D object detection benchmarks: ARKitScenes [3], the SpatialLM Dataset, and Structured3D [82]. Integrating SoPE yields consistent improvements on all datasets (Tables 2 and 3): on ARKitScenes, IoU<sub>3D</sub> F1@0.25/@0.50 improves by +2.2/+2.5; on the SpatialLM Dataset by +1.7/+1.4; and on Structured3D by +1.5/+0.3. These gains, particularly under looser IoU thresholds, support that SoPE’s hierarchical, geometry-aware encoding better captures positional information and directional variations in point-cloud tokens, leading to stronger 3D spatial understanding.

#### Comparison of different positional encoding methods.

As shown in Table 4, we evaluate three representative RoPE-based multimodal variants CCA, MCA, and RoPE-3D against our method to highlight the advantages of SpatialSoPE. CCA and MCA first project visual token indices onto a 2D plane and apply heuristic reassignment rules: CCA arranges indices in a communication-square pattern that increases from the boundary inward, while MCA computes indices directly from 2D spatial coordinates. In our reproduction, we extend these strategies to the 3D setting by projecting point-cloud tokens onto a 2D plane and applying analogous index reassignments. However, as the table shows, both methods yield suboptimal performance, likely because collapsing 3D structures into 2D discards crucial spatial locality and directional information. RoPE-3D, in



Figure 5. **Visualization of improvements in 3D object detection with SpatialSoPE.** Compared to SpatialLM, our method demonstrates significantly improved localization and sizing of 3D bounding boxes across various scenes.

Table 4. **Analysis of Component Contributions.** We demonstrate the impact of each key module by comparing the full SpatialSoPE model against the baseline and its intermediate variants on the ARKitScenes and SpatialLM datasets.

Methods	F1 - ARKitScenes		F1 - SpatialLM Dataset	
	IoU <sub>3D</sub> @0.25 <sup>↑</sup>	IoU <sub>3D</sub> @0.50 <sup>↑</sup>	IoU <sub>3D</sub> @0.25 <sup>↑</sup>	IoU <sub>3D</sub> @0.50 <sup>↑</sup>
SpatialLM [45]	63.9	60.7	69.7	62.0
+MCA [80]	63.7	60.2	70.1	61.6
+CCA [63]	64.1	60.5	69.8	62.5
+RoPE-3D	64.2	61.4	69.7	62.4
SpatialSoPE	<b>66.1</b>	<b>63.2</b>	<b>71.4</b>	<b>63.4</b>

contrast, shows that direct spatial encoding is a more effective paradigm, improving the IoU<sub>3D</sub>@0.50 F1 score from 60.7 to 61.4 by explicitly incorporating 3D coordinates.

Compared with the above methods, the proposed SpatialSoPE integrates a SoPE module that projects point cloud tokens into a 3D spherical coordinate space, jointly encoding spatial positions and directional angles. This geometry-aware positional encoding better matches the inherent 3D structure of point clouds, enhancing spatial awareness and improving IoU<sub>3D</sub> F1 to 66.1 and 63.2 at thresholds 0.25 and 0.50, respectively. A qualitative comparison is provided in Figure. 4.

Table 5. **Ablation study for our proposed SpatialSoPE method.** We validate our parameter choices by comparing against several variants on the ARKitScenes dataset.

Methods	$t : r : \theta : \phi$	F1 - ARKitScenes	
		IoU <sub>3D</sub> @0.25 <sup>↑</sup>	IoU <sub>3D</sub> @0.50 <sup>↑</sup>
Angular-Biased	(8:6:9:9)	65.5	62.7
Uniform	(1:1:1:1)	63.0	59.0
Temporal-Biased	(5:1:1:1)	65.0	62.7
SpatialSoPE	(24:2:3:3)	<b>66.1</b>	<b>63.2</b>

Table 6. **Effect of Multi-scale Frequency Mixing Strategy for RoPE-3D and SpatialSoPE.** We compare RoPE-3D and SpatialSoPE with and without the proposed Multi-scale Frequency Mixing Strategy, reporting F1 scores on ARKitScenes and the SpatialLM dataset.

Method	Multi-scale	F1 - ARKitScenes		F1 - SpatialLM Dataset	
		IoU <sub>3D</sub> @0.25 <sup>↑</sup>	IoU <sub>3D</sub> @0.50 <sup>↑</sup>	IoU <sub>3D</sub> @0.25 <sup>↑</sup>	IoU <sub>3D</sub> @0.50 <sup>↑</sup>
SpatialLM+RoPE-3D	×	64.2	<b>61.7</b>	69.4	62.3
	✓	64.8	62.1	70.3	62.9
SpatialSoPE	×	<b>65.4</b>	61.4	<b>71.0</b>	<b>62.5</b>
	✓	<b>66.1</b>	<b>63.2</b>	<b>71.4</b>	<b>63.4</b>

### 5.3. Ablation Studies

**Comparison of Frequency Allocation Schemes.** Under identical settings, we perform a controlled study that varies only the frequency allocation strategy in SpatialSoPE. As shown in Table 5, our allocation consistently outperforms all alternatives, suggesting that overemphasizing temporal frequencies harms geometric and orientation modeling, while overemphasizing angular/spatial frequencies undermines sequence-level stability. By reserving low-frequency capacity for long-range temporal coherence and assigning high-frequency bandwidth to spherical components, SpatialSoPE more accurately separates local from global 3D structure.

**Comparison of Multi-scale Frequency Mixing Strategy.** As shown in Table 6, we further evaluate the Multi-scale Frequency Mixing Strategy on both SpatialLM+RoPE-3D and SpatialSoPE. For SpatialLM+RoPE-3D, although  $(x, y, z)$  are encoded in Cartesian coordinates, multi-scale mixing brings only modest gains and mainly acts as a smoothing operation. In contrast, the same design yields clearly larger improvements for SpatialSoPE, where coarse scales preserve global layout and temporal stability, and fine scales emphasize small objects, boundaries, and orientation differences. Built on top of spherical reparameterization and tailored frequency allocation, the multi-scale strategy allows SpatialSoPE to better disentangle local and global 3D structure, leading to more stable detection and more accurate spatial perception.

### 5.4. Case Study

As illustrated in Figure 5, we present a qualitative comparison of 3D object detection performance across three different point cloud sources. The figure horizontally displays five viewpoints for each scene to dissect the effect of SpatialSoPE. A direct visual comparison shows that the model equipped with SoPE substantially reduces false detections, particularly for objects that are small or geometrically intricate, thereby improving overall robustness. In addition, SpatialSoPE further strengthens the model’s sensitivity to orientation and angular cues, leading to more consistent detection results across multiple views of the same scene. Taken together, these qualitative visualizations, along with the quantitative evaluations presented above, provide strong evidence that SpatialSoPE significantly enhances the model’s spatial perception and cross-view understanding in 3D environments.

### 5.5. Real-World Validation

SpatialSoPE’s strong spatial understanding of indoor environments has the potential to significantly advance embodied intelligence. To demonstrate its practical utility, we integrate SpatialSoPE into a complete robotic system and conduct real-world experiments, as illustrated in Fig. 6. First,



Figure 6. The figure illustrates the real-world experimental environment and the physical robot used in our study. Equipped with SpatialSoPE, the robot is capable of understanding the entire scene and executing exploration and object-transport tasks according to human instructions.

we reconstruct and render a point cloud of the environment using MAST3R-SLAM [46]. Next, SpatialSoPE processes the reconstructed scene to produce semantic labels, bounding boxes, and other object-level information. This information is then converted into a textual scene graph, from which we generate navigation target points—following a design similar to Work [20, 44, 50]—based on the bounding boxes of each piece of furniture for global path planning. Finally, inspired by Work [37, 72], we employ LLMs as the robot’s high-level task planner, encapsulating navigation, grasping, placing, and other behaviors into atomic actions. Built upon SpatialSoPE’s scene understanding, this enables general and efficient task planning for the robot. More details are provided in the supplementary material.

## 6. Conclusion

In this work, we proposed SoPE, a spherical orientation positional encoding tailored for 3D LVLMs that reparameterizes tokens in the  $(t : r : \theta : \phi)$  space, redistributes RoPE frequencies across temporal and angular dimensions, and performs multi-scale phase mixing to better capture 3D geometry and direction. Instantiated as a drop-in replacement for RoPE in SpatialLM, the resulting SpatialSoPE model achieves consistent gains on 3D layout estimation and 3D object detection benchmarks, while controlled ablations verify the contribution of the spherical reparameterization, frequency allocation strategy, and multi-scale phase mixing individually. Qualitative analyses further show that SpatialSoPE reduces false detections on small and geometrically intricate objects and yields more consistent predictions across multiple viewpoints of the same scene, indicating improved spatial perception and cross-view reasoning. Finally, we demonstrate that SpatialSoPE can be deployed in a real-world robotic system, providing rich scene-understanding signals for robot planning and validating its feasibility and superiority.

## References

- [1] Josh Achiam, Steven Adler, Sandhini Agarwal, Lama Ahmad, Ilge Akkaya, Florencia Leoni Aleman, Diogo Almeida, Janko Altenschmidt, Sam Altman, Shyamal Anadkat, et al. Gpt-4 technical report. *arXiv preprint arXiv:2303.08774*, 2023. 1
- [2] Armen Avetisyan, Christopher Xie, Henry Howard-Jenkins, Tsun-Yi Yang, Samir Aroudj, Suvam Patra, Fuyang Zhang, Duncan Frost, Luke Holland, Campbell Orme, et al. Scene-script: Reconstructing scenes with an autoregressive structured language model. In *European Conference on Computer Vision*, pages 247–263. Springer, 2024. 6
- [3] Gilad Baruch, Zhuoyuan Chen, Afshin Dehghan, Tal Dimry, Yuri Feigin, Peter Fu, Thomas Gebauer, Brandon Joffe, Daniel Kurz, Arik Schwartz, et al. Arkitscenes: A diverse real-world dataset for 3d indoor scene understanding using mobile rgb-d data. *arXiv preprint arXiv:2111.08897*, 2021. 6
- [4] Ananta R Bhattarai, Matthias Nießner, and Artem Sevastopolsky. Triplanenet: An encoder for eg3d inversion. In *Proceedings of the IEEE/CVF Winter Conference on Applications of Computer Vision*, pages 3055–3065, 2024. 1
- [5] Yuhang Cai, Jingfeng Wu, Song Mei, Michael Lindsey, and Peter Bartlett. Large stepsize gradient descent for non-homogeneous two-layer networks: Margin improvement and fast optimization. *Advances in Neural Information Processing Systems*, 37:71306–71351, 2024. 6
- [6] Boyuan Chen, Zhuo Xu, Sean Kirmani, Brain Ichter, Dorsa Sadigh, Leonidas Guibas, and Fei Xia. Spatialvlm: Endowing vision-language models with spatial reasoning capabilities. In *Proceedings of the IEEE/CVF Conference on Computer Vision and Pattern Recognition*, pages 14455–14465, 2024. 2
- [7] Junhao Chen, Xiang Li, Xiaojun Ye, Chao Li, Zhaoxin Fan, and Hao Zhao. Idea23d: Collaborative lmm agents enable 3d model generation from interleaved multimodal inputs. In *Proceedings of the 31st International Conference on Computational Linguistics*, pages 4149–4166, 2025.
- [8] Sijin Chen, Xin Chen, Chi Zhang, Mingsheng Li, Gang Yu, Hao Fei, Hongyuan Zhu, Jiayuan Fan, and Tao Chen. Ll3da: Visual interactive instruction tuning for omni-3d understanding reasoning and planning. In *Proceedings of the IEEE/CVF conference on computer vision and pattern recognition*, pages 26428–26438, 2024. 1, 2
- [9] Yuhan Chen, Ang Lv, Jian Luan, Bin Wang, and Wei Liu. Hope: A novel positional encoding without long-term decay for enhanced context awareness and extrapolation. *arXiv preprint arXiv:2410.21216*, 2024. 2
- [10] An-Chieh Cheng, Hongxu Yin, Yang Fu, Qiushan Guo, Ruihan Yang, Jan Kautz, Xiaolong Wang, and Sifei Liu. Spatial-rgpt: Grounded spatial reasoning in vision-language models. *Advances in Neural Information Processing Systems*, 37:135062–135093, 2024. 1
- [11] Junda Cheng, Wei Yin, Kaixuan Wang, Xiaozhi Chen, Shijie Wang, and Xin Yang. Adaptive fusion of single-view and multi-view depth for autonomous driving. In *Proceedings of the IEEE/CVF Conference on Computer Vision and Pattern Recognition*, pages 10138–10147, 2024. 1
- [12] Erik Daxberger, Nina Wenzel, David Griffiths, Haiming Gang, Justin Lazarow, Gefen Kohavi, Kai Kang, Marcin Eichner, Yinfei Yang, Afshin Dehghan, et al. Mm-spatial: Exploring 3d spatial understanding in multimodal llms. In *Proceedings of the IEEE/CVF International Conference on Computer Vision*, pages 7395–7408, 2025. 2
- [13] Xiaohan Ding, Yiyuan Zhang, Yixiao Ge, Sijie Zhao, Lin Song, Xiangyu Yue, and Ying Shan. Unireplknet: A universal perception large-kernel convnet for audio video point cloud time-series and image recognition. In *Proceedings of the IEEE/CVF conference on computer vision and pattern recognition*, pages 5513–5524, 2024. 1
- [14] Zhipeng Ding, Xu Han, and Marc Niethammer. Votenet: A deep learning label fusion method for multi-atlas segmentation. In *International conference on medical image computing and computer-assisted intervention*, pages 202–210. Springer, 2019. 6
- [15] Xiaoqi Dong, Xiangyu Zhou, Nicholas Evans, and Yujia Lin. Lumigen: An lvm-enhanced iterative framework for fine-grained text-to-image generation. *arXiv preprint arXiv:2508.04732*, 2025. 2
- [16] Jinyong Fan and Yanyan Shen. Stockmixer: A simple yet strong mlp-based architecture for stock price forecasting. In *Proceedings of the AAI conference on artificial intelligence*, pages 8389–8397, 2024. 6
- [17] Zhiwen Fan, Jian Zhang, Renjie Li, Junge Zhang, Runjin Chen, Hezhen Hu, Kevin Wang, Huaizhi Qu, Dilin Wang, Zhicheng Yan, et al. Vlm-3r: Vision-language models augmented with instruction-aligned 3d reconstruction. *arXiv preprint arXiv:2505.20279*, 2025. 2
- [18] Yu Gan, Yunning You, Junjie Huang, Sen Xiang, Chang Tang, Wei Hu, and Shan An. Multi-view clustering via multi-stage fusion. *IEEE Transactions on Multimedia*, 2025. 1
- [19] Ge Gao, Alexey Taymanov, Eduardo Salinas, Paul Mineiro, and Dipendra Misra. Aligning llm agents by learning latent preference from user edits. *Advances in Neural Information Processing Systems*, 37:136873–136896, 2024. 2
- [20] Jiayuan Gu, Devendra Singh Chaplot, Hao Su, and Jitendra Malik. Multi-skill mobile manipulation for object rearrangement. *arXiv preprint arXiv:2209.02778*, 2022. 8
- [21] Meilan Hao, Zhongkang Zhang, Lei Li, Kejian Dong, Long Cheng, Prayag Tiwari, and Xin Ning. Coarse to fine-based image–point cloud fusion network for 3d object detection. *Information Fusion*, 112:102551, 2024. 1
- [22] Byeongho Heo, Song Park, Dongyoon Han, and Sangdoon Yun. Rotary position embedding for vision transformer. In *European Conference on Computer Vision*, pages 289–305. Springer, 2024. 1, 2
- [23] Georg Hess, Adam Tonderski, Christoffer Petersson, Kalle Åström, and Lennart Svensson. Lidarclip or: How i learned to talk to point clouds. In *Proceedings of the IEEE/CVF Winter Conference on Applications of Computer Vision*, pages 7438–7447, 2024. 1
- [24] Yining Hong, Haoyu Zhen, Peihao Chen, Shuhong Zheng, Yilun Du, Zhenfang Chen, and Chuang Gan. 3d-llm: Injecting the 3d world into large language models. *Advances*

- in *Neural Information Processing Systems*, 36:20482–20494, 2023. 1, 2
- [25] Hanzhe Hu, Zhizhuo Zhou, Varun Jampani, and Shubham Tulsiani. Mvd-fusion: Single-view 3d via depth-consistent multi-view generation. In *Proceedings of the IEEE/CVF Conference on Computer Vision and Pattern Recognition*, pages 9698–9707, 2024. 1
- [26] Kai Hu, Feng Gao, Xiaohan Nie, Peng Zhou, Son Tran, Tal Neiman, Lingyun Wang, Mubarak Shah, Raffay Hamid, Bing Yin, et al. M-llm based video frame selection for efficient video understanding. In *Proceedings of the Computer Vision and Pattern Recognition Conference*, pages 13702–13712, 2025. 1
- [27] Wenbo Hu, Yining Hong, Yanjun Wang, Leison Gao, Zibu Wei, Xingcheng Yao, Nanyun Peng, Yonatan Bitton, Idan Szpektor, and Kai-Wei Chang. 3dllm-mem: Long-term spatial-temporal memory for embodied 3d large language model. *arXiv preprint arXiv:2505.22657*, 2025. 2
- [28] Yutao Hu, Tianbin Li, Quanfeng Lu, Wenqi Shao, Junjun He, Yu Qiao, and Ping Luo. Omnimedvqa: A new large-scale comprehensive evaluation benchmark for medical lvlm. In *Proceedings of the IEEE/CVF Conference on Computer Vision and Pattern Recognition*, pages 22170–22183, 2024. 2
- [29] Ermo Hua, Che Jiang, Xingtai Lv, Kaiyan Zhang, Youbang Sun, Yuchen Fan, Xuekai Zhu, Biqing Qi, Ning Ding, and Bowen Zhou. Fourier position embedding: Enhancing attention’s periodic extension for length generalization. *arXiv preprint arXiv:2412.17739*, 2024. 2
- [30] Hsiang-Wei Huang, Fu-Chen Chen, Wenhao Chai, Che-Chun Su, Lu Xia, Sanghun Jung, Cheng-Yen Yang, Jenq-Neng Hwang, Min Sun, and Cheng-Hao Kuo. Zero-shot 3d question answering via voxel-based dynamic token compression. In *Proceedings of the Computer Vision and Pattern Recognition Conference*, pages 19424–19434, 2025. 2
- [31] Hang Ji, Tao Ni, Xufeng Huang, Zhan Shi, Tao Luo, Xin Zhan, and Junbo Chen. Ropetr: Improving temporal camera-only 3d detection by integrating enhanced rotary position embedding. *arXiv preprint arXiv:2504.12643*, 2025. 2
- [32] Li Jiang, Shaoshuai Shi, and Bernt Schiele. Open-vocabulary 3d semantic segmentation with foundation models. In *Proceedings of the IEEE/CVF Conference on Computer Vision and Pattern Recognition*, pages 21284–21294, 2024. 2
- [33] Xin Jin, Haisheng Su, Cong Ma, Kai Liu, Wei Wu, Fei Hui, and Junchi Yan. Geoformer: Geometry point encoder for 3d object detection with graph-based transformer. In *Proceedings of the IEEE/CVF International Conference on Computer Vision*, pages 26879–26889, 2025. 1
- [34] Muhammad Uzair Khattak, Muhammad Ferjad Naeem, Jameel Hassan, Muzammal Naseer, Federico Tombari, Fahad Shahbaz Khan, and Salman Khan. How good is my video-lmm? complex video reasoning and robustness evaluation suite for video-lmms. In *Proceedings of the Computer Vision and Pattern Recognition Conference*, pages 3642–3651, 2025. 2
- [35] Maksim Kolodiazhyi, Anna Vorontsova, Matvey Skripkin, Danila Rukhovich, and Anton Konushin. Unidet3d: Multi-dataset indoor 3d object detection. In *Proceedings of the AAAI Conference on Artificial Intelligence*, pages 4365–4373, 2025. 6
- [36] Zechuan Li, Hongshan Yu, Yihao Ding, Shuai Yuan, and Naveed Akhtar. Lpl3d: Lvlm-driven pseudo-labeling for 3d object detection. *IEEE Transactions on Circuits and Systems for Video Technology*, 2025. 2
- [37] Kehui Liu, Zixin Tang, Dong Wang, Zhigang Wang, Xuelong Li, and Bin Zhao. Coherent: Collaboration of heterogeneous multi-robot system with large language models. In *IEEE International Conference on Robotics and Automation (ICRA)*, pages 10208–10214. IEEE, 2025. 8, 1
- [38] Shi Liu, Weijie Su, Xizhou Zhu, Wenhai Wang, and Jifeng Dai. Comemo: Lvlms need image context with image memory. *arXiv preprint arXiv:2506.06279*, 2025. 2
- [39] Zhenyang Liu, Yikai Wang, Sixiao Zheng, Tongying Pan, Longfei Liang, Yanwei Fu, and Xiangyang Xue. Reasongrounder: Lvlm-guided hierarchical feature splatting for open-vocabulary 3d visual grounding and reasoning. In *Proceedings of the Computer Vision and Pattern Recognition Conference*, pages 3718–3727, 2025. 2
- [40] Jannik Lübberstedt, Esteban Rivera Guerrero, Nico Uhlemann, and Markus Lienkamp. V3lma: Visual 3d-enhanced language model for autonomous driving. In *Proceedings of the Computer Vision and Pattern Recognition Conference*, pages 4769–4778, 2025.
- [41] Ruiyuan Lyu, Jingli Lin, Tai Wang, Shuai Yang, Xiaohan Mao, Yilun Chen, Runsen Xu, Haifeng Huang, Chenming Zhu, Dahua Lin, et al. Mmscan: A multi-modal 3d scene dataset with hierarchical grounded language annotations. *Advances in Neural Information Processing Systems*, 37:50898–50924, 2024.
- [42] Wufei Ma, Haoyu Chen, Guofeng Zhang, Yu-Cheng Chou, Jieneng Chen, Celso de Melo, and Alan Yuille. 3dsrbench: A comprehensive 3d spatial reasoning benchmark. In *Proceedings of the IEEE/CVF International Conference on Computer Vision*, pages 6924–6934, 2025. 2
- [43] Wufei Ma, Luoxin Ye, Celso M de Melo, Alan Yuille, and Jieneng Chen. Spatialllm: A compound 3d-informed design towards spatially-intelligent large multimodal models. In *Proceedings of the Computer Vision and Pattern Recognition Conference*, pages 17249–17260, 2025. 2
- [44] Abhijit Makhhal and Alex K Goins. Reuleaux: Robot base placement by reachability analysis. In *2018 second IEEE international conference on robotic computing (IRC)*, pages 137–142. IEEE, 2018. 8
- [45] Yongsan Mao, Junhao Zhong, Chuan Fang, Jia Zheng, Rui Tang, Hao Zhu, Ping Tan, and Zihan Zhou. Spatialllm: Training large language models for structured indoor modeling. *ArXiv*, abs/2506.07491, 2025. 3, 6, 7
- [46] Riku Murai, Eric Dexheimer, and Andrew J Davison. Mast3r-slam: Real-time dense slam with 3d reconstruction priors. In *Proceedings of the Computer Vision and Pattern Recognition Conference*, pages 16695–16705, 2025. 8
- [47] Huantao Ren, Jiyang Wang, Minmin Yang, and Senem Velipasalar. Pointofview: A multi-modal network for few-shot 3d point cloud classification fusing point and multi-view image features. In *Proceedings of the IEEE/CVF conference on*

- computer vision and pattern recognition*, pages 784–793, 2024. 1
- [48] Yazhou Ren, Xinyue Chen, Jie Xu, Jingyu Pu, Yonghao Huang, Xiaorong Pu, Ce Zhu, Xiaofeng Zhu, Zhifeng Hao, and Lifang He. A novel federated multi-view clustering method for unaligned and incomplete data fusion. *Information Fusion*, 108:102357, 2024. 1
- [49] J. Su, M. Ahmed, Y. Lu, S. Pan, W. Bo, and Y. Liu. Ro-former: Enhanced transformer with rotary position embedding. *Neurocomputing*, 568:127063, 2024. 1
- [50] Andrew Szot, Karmesh Yadav, Alex Clegg, Vincent-Pierre Berges, Aaron Gokaslan, Angel Chang, Manolis Savva, Zsolt Kira, and Dhruv Batra. Habitat rearrangement challenge 2022, 2022. 8
- [51] Yiwen Tang, Ray Zhang, Jiaming Liu, Zoey Guo, Bin Zhao, Zhigang Wang, Peng Gao, Hongsheng Li, Dong Wang, and Xuelong Li. Any2point: Empowering any-modality large models for efficient 3d understanding. In *European Conference on Computer Vision*, pages 456–473. Springer, 2024. 1
- [52] Diantao Tu, Hainan Cui, Xianwei Zheng, and Shuhan Shen. Panopose: Self-supervised relative pose estimation for panoramic images. In *Proceedings of the IEEE/CVF Conference on Computer Vision and Pattern Recognition*, pages 20009–20018, 2024. 2
- [53] Chengcheng Wang, Jianyuan Guo, Hongguang Li, Yuchuan Tian, Ying Nie, Chang Xu, and Kai Han. Circle-rope: Cone-like decoupled rotary positional embedding for large vision-language models. *arXiv preprint arXiv:2505.16416*, 2025. 3
- [54] Han Wang, Yuxiang Nie, Yongjie Ye, Yanjie Wang, Shuai Li, Haiyang Yu, Jinghui Lu, and Can Huang. Dynamic-vlm: Simple dynamic visual token compression for videollm. In *Proceedings of the IEEE/CVF International Conference on Computer Vision*, pages 20812–20823, 2025. 2
- [55] Jiarui Wang, Huiyu Duan, Guangtao Zhai, Juntong Wang, and Xionghuo Min. Aigv-assessor: benchmarking and evaluating the perceptual quality of text-to-video generation with lmm. In *Proceedings of the Computer Vision and Pattern Recognition Conference*, pages 18869–18880, 2025. 2
- [56] Peng Wang, Shuai Bai, Sinan Tan, Shijie Wang, Zhihao Fan, Jinze Bai, Keqin Chen, Xuejing Liu, Jialin Wang, Wenbin Ge, et al. Qwen2-vl: Enhancing vision-language model’s perception of the world at any resolution. *arXiv preprint arXiv:2409.12191*, 2024. 2
- [57] Qihang Wang, Xiaoming Wang, Qing He, Jun Huang, Hong Huang, Ping Wang, Tianle Yu, and Min Zhang. 3d tensor-based point cloud and image fusion for robust detection and measurement of rail surface defects. *Automation in Construction*, 161:105342, 2024. 1
- [58] Zehan Wang, Haifeng Huang, Yang Zhao, Ziang Zhang, and Zhou Zhao. Chat-3d: Data-efficiently tuning large language model for universal dialogue of 3d scenes. *arXiv preprint arXiv:2308.08769*, 2023. 1
- [59] Xilin Wei, Xiaoran Liu, Yuhang Zang, Xiaoyi Dong, Pan Zhang, Yuhang Cao, Jian Tong, Haodong Duan, Qipeng Guo, Jiaqi Wang, et al. Videorope: What makes for good video rotary position embedding? *arXiv preprint arXiv:2502.05173*, 2025. 2
- [60] Shuang Wu, Youtian Lin, Feihu Zhang, Yifei Zeng, Jingxi Xu, Philip Torr, Xun Cao, and Yao Yao. Direct3d: Scalable image-to-3d generation via 3d latent diffusion transformer. *Advances in Neural Information Processing Systems*, 37:121859–121881, 2024. 1
- [61] Xiaoyang Wu, Daniel DeTone, Duncan Frost, Tianwei Shen, Chris Xie, Nan Yang, Jakob Julian Engel, Richard A. Newcombe, Hengshuang Zhao, and Julian Straub. Sonata: Self-supervised learning of reliable point representations. *2025 IEEE/CVF Conference on Computer Vision and Pattern Recognition (CVPR)*, pages 22193–22204, 2025. 6
- [62] Jinsheng Xiao, Shurui Wang, Jian Zhou, Ziyue Tian, Hongping Zhang, and Yuan-Fang Wang. Mim: High-definition maps incorporated multi-view 3d object detection. *IEEE Transactions on Intelligent Transportation Systems*, 2024. 1
- [63] Yun Xing, Yiheng Li, Ivan Laptev, and Shijian Lu. Mitigating object hallucination via concentric causal attention. *Advances in neural information processing systems*, 37:92012–92035, 2024. 7
- [64] Chenfeng Xu, Bichen Wu, Ji Hou, Sam Tsai, Ruilong Li, Jialiang Wang, Wei Zhan, Zijian He, Peter Vajda, Kurt Keutzer, et al. Nerf-det: Learning geometry-aware volumetric representation for multi-view 3d object detection. In *Proceedings of the IEEE/CVF International Conference on Computer Vision*, pages 23320–23330, 2023. 6
- [65] Runsen Xu, Xiaolong Wang, Tai Wang, Yilun Chen, Jiangmiao Pang, and Dahua Lin. Pointllm: Empowering large language models to understand point clouds. In *European Conference on Computer Vision*, pages 131–147. Springer, 2024. 1, 2
- [66] Xiangyuan Xue, Zeyu Lu, Di Huang, Zidong Wang, Wanli Ouyang, and Lei Bai. Comfybench: Benchmarking llm-based agents in comfyui for autonomously designing collaborative ai systems. In *Proceedings of the Computer Vision and Pattern Recognition Conference*, pages 24614–24624, 2025. 1
- [67] Qianqi Yan, Xuehai He, and Xin Eric Wang. Med-hvl: Automatic medical domain hallucination evaluation for large vision-language models. In *AAAI 2024 Spring Symposium on Clinical Foundation Models*, 2024. 2
- [68] Qwen An Yang, Baosong Yang, Beichen Zhang, Binyuan Hui, Bo Zheng, Bowen Yu, Chengyuan Li, Dayiheng Liu, Fei Huang, Guanting Dong, Haoran Wei, Huan Lin, Jian Yang, Jianhong Tu, Jianwei Zhang, Jianxin Yang, Jiaxin Yang, Jingren Zhou, Junyang Lin, Kai Dang, Keming Lu, Keqin Bao, Kexin Yang, Le Yu, Mei Li, Mingfeng Xue, Pei Zhang, Qin Zhu, Rui Men, Runji Lin, Tianhao Li, Tingyu Xia, Xingzhang Ren, Xuancheng Ren, Yang Fan, Yang Su, Yi-Chao Zhang, Yunyang Wan, Yuqi Liu, Zeyu Cui, Zhenru Zhang, Zihan Qiu, Shanghaoran Quan, and Zekun Wang. Qwen2.5 technical report. *ArXiv*, abs/2412.15115, 2024. 6
- [69] Hao Yu, Tangyu Jiang, Shuning Jia, Shannan Yan, Shunning Liu, Haolong Qian, Guanghao Li, Shuting Dong, and Chun Yuan. Comrope: Scalable and robust rotary position embedding parameterized by trainable commuting angle matrices.

- In *Proceedings of the Computer Vision and Pattern Recognition Conference*, pages 4508–4517, 2025. 2
- [70] Hanxun Yu, Wentong Li, Song Wang, Junbo Chen, and Jianke Zhu. Inst3d-lmm: Instance-aware 3d scene understanding with multi-modal instruction tuning. In *Proceedings of the Computer Vision and Pattern Recognition Conference*, pages 14147–14157, 2025. 2
- [71] Tianyu Yu, Zefan Wang, Chongyi Wang, Fuwei Huang, Wenshuo Ma, Zhihui He, Tianchi Cai, Weize Chen, Yuxiang Huang, Yuanqian Zhao, et al. Minicpm-v 4.5: Cooking efficient mllms via architecture, data, and training recipe. *arXiv preprint arXiv:2509.18154*, 2025. 2
- [72] Wenhao Yu, Jie Peng, Yueliang Ying, Sai Li, Jianmin Ji, and Yanyong Zhang. Mhrc: Closed-loop decentralized multi-heterogeneous robot collaboration with large language models. *arXiv preprint arXiv:2409.16030*, 2024. 8, 1
- [73] Zhu Yu, Bowen Pang, Lizhe Liu, Runmin Zhang, Qiang Li, Si-Yuan Cao, Maochun Luo, Mingxia Chen, Sheng Yang, and Hui-Liang Shen. Language driven occupancy prediction. In *Proceedings of the IEEE/CVF International Conference on Computer Vision*, pages 7548–7558, 2025. 2
- [74] Yuanwen Yue, Theodora Kontogianni, Konrad Schindler, and Francis Engelmann. Connecting the dots: Floorplan reconstruction using two-level queries. In *Proceedings of the IEEE/CVF conference on computer vision and pattern recognition*, pages 845–854, 2023. 6
- [75] Tatiana Zemskova and Dmitry Yudin. 3dgraphllm: Combining semantic graphs and large language models for 3d scene understanding. In *Proceedings of the IEEE/CVF International Conference on Computer Vision*, pages 8885–8895, 2025. 2
- [76] Shaofeng Zhang, Qiang Zhou, Sitong Wu, Haoru Tan, Zhibin Wang, Jinfa Huang, and Junchi Yan. Cr2pq: Continuous relative rotary positional query for dense visual representation learning. In *The Thirteenth International Conference on Learning Representations*. 3
- [77] Xuying Zhang, Yutong Liu, Yangguang Li, Renrui Zhang, Yufei Liu, Kai Wang, Wanli Ouyang, Zhiwei Xiong, Peng Gao, Qibin Hou, et al. Tar3d: Creating high-quality 3d assets via next-part prediction. In *Proceedings of the IEEE/CVF International Conference on Computer Vision*, pages 5134–5145, 2025. 1
- [78] Zaiwei Zhang, Bo Sun, Haitao Yang, and Qixing Huang. H3dnet: 3d object detection using hybrid geometric primitives. In *European conference on computer vision*, pages 311–329. Springer, 2020. 6
- [79] Jianbo Zhao, Taiyu Ban, Zhihao Liu, Hangning Zhou, Xiyang Wang, Qibin Zhou, Hailong Qin, Mu Yang, Lei Liu, and Bin Li. Drope: Directional rotary position embedding for efficient agent interaction modeling. *arXiv preprint arXiv:2503.15029*, 2025. 3
- [80] Qiyan Zhao, Xiaofeng Zhang, Yiheng Li, Yun Xing, Xiaosong Yuan, Feilong Tang, Sinan Fan, Xuhang Chen, Xuyao Zhang, and Dahan Wang. Mca-llava: Manhattan causal attention for reducing hallucination in large vision-language models. *arXiv preprint arXiv:2507.09184*, 2025. 2, 7
- [81] Duo Zheng, Shijia Huang, and Liwei Wang. Video-3d llm: Learning position-aware video representation for 3d scene understanding. In *Proceedings of the Computer Vision and Pattern Recognition Conference*, pages 8995–9006, 2025. 1
- [82] Jia Zheng, Junfei Zhang, Jing Li, Rui Tang, Shenghua Gao, and Zihan Zhou. Structured3d: A large photo-realistic dataset for structured 3d modeling. In *European Conference on Computer Vision*, pages 519–535. Springer, 2020. 6
- [83] Hongyan Zhi, Peihao Chen, Junyan Li, Shuailei Ma, Xinyu Sun, Tianhang Xiang, Yinjie Lei, Mingkui Tan, and Chuang Gan. Lscenellm: Enhancing large 3d scene understanding using adaptive visual preferences. *arXiv preprint arXiv:2412.01292*, 2024. 1
- [84] Hongyan Zhi, Peihao Chen, Junyan Li, Shuailei Ma, Xinyu Sun, Tianhang Xiang, Yinjie Lei, Mingkui Tan, and Chuang Gan. Lscenellm: Enhancing large 3d scene understanding using adaptive visual preferences. In *Proceedings of the Computer Vision and Pattern Recognition Conference*, pages 3761–3771, 2025. 2
- [85] Hanyu Zhou and Gim Hee Lee. Llava-4d: Embedding spatiotemporal prompt into llms for 4d scene understanding. *arXiv preprint arXiv:2505.12253*, 2025. 2
- [86] Chenming Zhu, Tai Wang, Wenwei Zhang, Jiangmiao Pang, and Xihui Liu. Llava-3d: A simple yet effective pathway to empowering llms with 3d-awareness. *arXiv preprint arXiv:2409.18125*, 2024. 1
- [87] Fangrui Zhu, Hanhui Wang, Yiming Xie, Jing Gu, Tianye Ding, Jianwei Yang, and Huaizu Jiang. Struct2d: A perception-guided framework for spatial reasoning in large multimodal models. *arXiv preprint arXiv:2506.04220*, 2025. 2
- [88] Lei Zhu, Fangyun Wei, and Yanye Lu. Beyond text: Frozen large language models in visual signal comprehension. In *Proceedings of the IEEE/CVF Conference on Computer Vision and Pattern Recognition*, pages 27047–27057, 2024. 1
- [89] Orr Zohar, Xiaohan Wang, Yann Dubois, Nikhil Mehta, Tong Xiao, Philippe Hansen-Estruch, Licheng Yu, Xiaofang Wang, Felix Juefei-Xu, Ning Zhang, et al. Apollo: An exploration of video understanding in large multimodal models. In *Proceedings of the Computer Vision and Pattern Recognition Conference*, pages 18891–18901, 2025. 1
- [90] Qi Zuo, Xiaodong Gu, Yuan Dong, Zhengyi Zhao, Weihao Yuan, Lingteng Qiu, Liefeng Bo, and Zilong Dong. High-fidelity 3d textured shapes generation by sparse encoding and adversarial decoding. In *European Conference on Computer Vision*, pages 52–69. Springer, 2024. 1

# SoPE: Spherical Coordinate-Based Positional Embedding for Enhancing Spatial Perception of 3D LLMs

## Supplementary Material



Figure 7. Detection visualization and task environments of SpatialSoPE in real-world reconstructed scenes.

## 7. Real-World Validation

### 7.1. Settings

In this section, we present a detailed account of the real-robot experimental validation process. Fig. 7 illustrates the reconstructed scene point cloud, the model’s visual outputs, and the corresponding real-world setup. We build a simulated indoor home environment containing a table, sofa, bookshelf, refrigerator, and other common furniture. The experimental platform is the Galaxea R1 Lite mobile dual-arm robot, equipped with a wrist-mounted RealSense D435i, a RealSense D455, and a Mid-360 LiDAR. We design distinct atomic action sets for the robot to encapsulate its physical capabilities, including:

1. [navigate] to `<stand_pose_id>` of `<object>`;
2. [open] `<container>`;
3. [pick] up `<object>`;
4. [place] `<object>` on/into `<platform>`;
5. [move] `<delta.x>` and `<delta.y>`;

Following the methodologies of prior work [37, 72], we employ LLM-based role-playing to guide task planning through a Chain-of-Thought (CoT) framework. The robot selects and executes one action at a time from a predefined list. After each action, it receives feedback and, using this information together with its execution history, autonomously determines the next subtask or adjusts its plan. This multi-turn process enables effective coordination for long-horizon tasks. The detailed prompt design is provided in Subsection 7.2.

In the real-robot system, for manipulation tasks, we use AnyGrasp to predict grasp points and apply Grounded SAM to filter candidates based on semantic targets. The resulting grasp poses are executed via inverse-kinematics planning. For navigation tasks, we adopt a SLAM pipeline for mapping and localization, with A\* as the global planner and DWA as the local planner.

We further integrate the multimodal *GPT-4o* model to obtain scene understanding and action-level feedback in real-world environments. After each action, the manipulator’s wrist camera captures the current scene to assess execution success and overall task progress. For example, once the mobile robot reaches a new piece of furniture, *GPT-4o* identifies the objects on it to support exploration in unknown environments. Similarly, after each picking or placing operation, *GPT-4o* verifies whether the action was executed correctly. Additional feedback, such as pose estimation or inverse-kinematics results, can also be incorporated into the evaluation process.

### 7.2. Prompts

==== System Prompt ====

#### Role:

1. You are an intelligent robot named `_${name}`, configured with a wheeled chassis and a single manipulator arm.
2. You possess the ability to navigate across the ground and perform manipulation tasks, including transporting various objects and opening hinged objects.

#### Skills:

1. `navigate(obj, pose)`; `open(obj)`;
2. `pick(obj)`; `place(obj, loc)`; `move(dx, dy)`;

#### Task Objective and Context:

1. The overall task is: `_${target_task}`.
2. Ingredients are scattered in an unknown indoor environment. The scene graph shows furniture locations but not their contents. Based on task goal, objects must be placed.

#### Principles:

1. Efficiently explore and navigate all locations in the scene graph without repetition.
2. Transport task-related items promptly.
3. Track task progress and adjust targets timely.
4. If grasp fails, try other stand poses or adjust base position.
5. Focus on completing the task without unrelated actions.

#### Output Response Format:

1. Thoughts: think step by step to analyze the problem;
2. Contents: choose and execute only one action from the action functions above.

#### CoT: Let’s think step by step!

**Examples:** The following examples are provided for reference in decision-making. The related content involved has nothing to do with the actual task: [...]

==== User Prompt ====

#### Scene Graph:

drawer: (pos: [...], ori: [...], state: close, stand: [...]),  
cabinet: (...), sofa: (...), ... (It is generated by SpatialSoPE)

#### Robot Status:

Current robot states: pos: [...], ori: [...]. The gripper is empty.

**Feedback History:**

The historical feedbacks, from oldest to newest, are as follows: [... Robot successfully reached the target book case-stand pose 0. ['book 0', 'book 1'] are found on the book case ...]

**Action History:**

The historical actions, from oldest to newest, are as follows: [... navigate(book case, stand pose 0) ...]